

Dissipative Softening of Chern Plateaus in a Two-Sector Lattice Dirac Model

Aaron Alderman

28 April 2026

Abstract

We study a two-band lattice Dirac model of Qi-Wu-Zhang type coupled to a Lindblad dephasing bath with jump operator $L = \sigma_z$. The main result is a closed-form dissipatively softened Hall response

$$\sigma_{xy}^{\text{eff}}(M, \gamma) = \frac{e^2}{h} \int_{\text{BZ}} \frac{d^2k}{2\pi} \Omega(k) \frac{4|d(k)|^2}{4|d(k)|^2 + \gamma^2},$$

in which dephasing suppresses spectral weight directly rather than acting through thermal occupation. This produces momentum-selective erosion of Chern plateaus that is strongest near local gap closures. The most distinctive prediction is a doubled-cusp enhancement at $M = 0$, where two high-symmetry gap closures contribute simultaneously, in contrast to the single-point closures at $M = \pm 2$. A numerical implementation and figure-generation scripts are included.

Keywords. topological insulators, Chern number, Lindblad master equation, Hall conductivity, dephasing, open quantum systems, QWZ model, Berry curvature

1 The Lattice Model: Qi-Wu-Zhang Hamiltonian

We work on a square lattice with Bloch Hamiltonian

$$H(k) = d(k) \cdot \sigma = d_x(k)\sigma_x + d_y(k)\sigma_y + d_z(k)\sigma_z,$$

where

$$d_x(k) = \sin k_x, \quad d_y(k) = \sin k_y, \quad d_z(k) = M + \cos k_x + \cos k_y.$$

The mass parameter M tunes topological transitions by closing the gap at special momenta: $\Gamma = (0, 0)$ for $M = -2$, $X = (\pi, 0)$ and $Y = (0, \pi)$ for $M = 0$, and (π, π) for $M = +2$.

Figure 1 - QWZ Band Structure at Topological Phase Boundaries

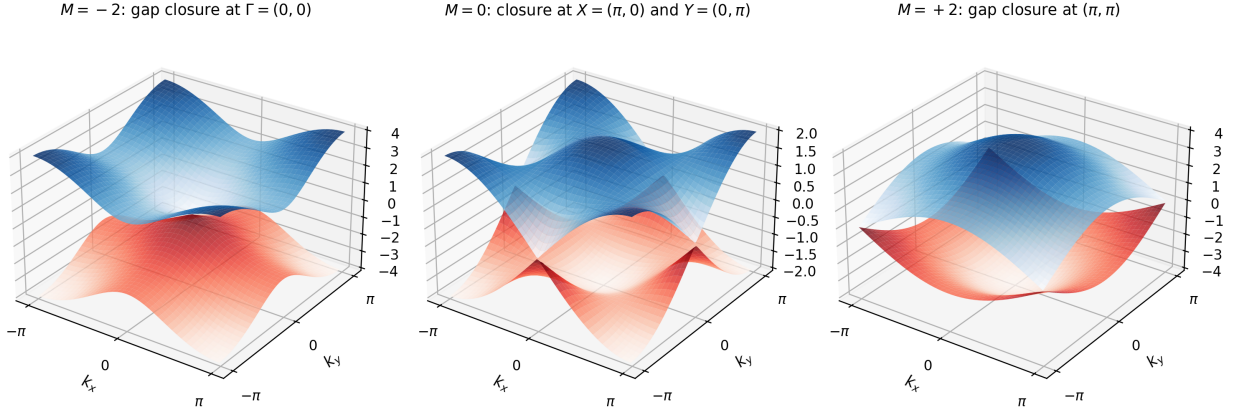


Figure 1: QWZ band structure at the three phase boundaries. The upper and lower bands $\pm|d(k)|$ touch at the corresponding high-symmetry points.

2 Topological Invariants: Berry Curvature and Chern Number

In the closed-system limit $\gamma = 0$, the band topology is encoded in the Berry curvature

$$\Omega(k) = \frac{1}{2} \frac{d \cdot (\partial_{k_x} d \times \partial_{k_y} d)}{|d|^3},$$

and the Chern number

$$C = \frac{1}{2\pi} \int_{\text{BZ}} \Omega(k) d^2k.$$

The phase diagram is

| Parameter range | Chern number | Phase |
|-----------------|--------------|-------------------|
| $-2 < M < 0$ | $C = +1$ | topological |
| $0 < M < 2$ | $C = -1$ | topological |
| $ M > 2$ | $C = 0$ | trivial insulator |

3 Dissipative Dynamics: Lindblad Dephasing

3.1 Physical justification of the jump operator

We model quasi-static fluctuations of the local gap parameter by the diagonal Lindblad jump operator

$$L = \sigma_z.$$

This is intended to capture crystal-field or strain fluctuations that shift the relative energy of the two orbital sectors without inducing coherent spin-flip transitions. In the weak-coupling, Markovian regime the reduced density matrix obeys

$$\dot{\rho} = -i[H, \rho] + \gamma(\sigma_z \rho \sigma_z - \rho).$$

The important conceptual point is that this dephasing term changes spectral weight directly. It therefore differs from thermal broadening, which modifies occupation numbers through the Fermi distribution.

4 Effective Hall Response: Derivation and Validity

4.1 Kubo-Bastin starting point

The Hall response is written in Kubo-Bastin form as

$$\sigma_{xy}^{\text{eff}} \propto \text{Tr} \int d\varepsilon f(\varepsilon) \left[v_x \frac{dG^R}{d\varepsilon} v_y (G^R - G^A) - v_x (G^R - G^A) v_y \frac{dG^A}{d\varepsilon} \right].$$

4.2 Self-energy approximation

Lindblad dephasing is incorporated by replacing the infinitesimal convergence factor $i\eta$ with a finite self-energy

$$\Sigma = i\gamma/2, \quad G^{R/A}(k, \varepsilon) = \frac{1}{\varepsilon - H(k) \pm i\gamma/2}.$$

This is a Born-level, momentum-independent approximation intended for $\gamma \ll W$ with W the bandwidth and with momentum-dependent disorder effects neglected.

4.3 Derivation of the damping factor

For the two-level system, the advanced/retarded pole structure produces the damping factor

$$\frac{E^2}{E^2 + (\gamma/2)^2} = \frac{4E^2}{4E^2 + \gamma^2},$$

where $E(k) = |d(k)|$. The factor of 4 is fixed by the two-pole trace algebra. This weight tends to 1 as $\gamma \rightarrow 0$ and to 0 when $E \rightarrow 0$ at fixed γ .

4.4 The softened Hall conductivity

Putting the ingredients together yields

$$\sigma_{xy}^{\text{eff}}(M, \gamma) = \frac{e^2}{h} \int_{\text{BZ}} \frac{d^2k}{2\pi} \Omega(k) \frac{4|d(k)|^2}{4|d(k)|^2 + \gamma^2}.$$

States deep inside a plateau remain nearly unaffected because $|d(k)|$ stays large across the Brillouin zone. States near a local gap closure are strongly suppressed because the same low-gap region carries the dominant Berry-curvature weight.

5 Phase Map and the Doubled Cusp Effect

5.1 Qualitative structure

The dissipative phase map exhibits three clearly separated regimes:

- plateau interiors, where $\sigma_{xy}^{\text{eff}} \approx \pm 1$ remains close to Chern quantization;
- single-point closures at $M = \pm 2$, which generate one cusp each;
- the doubled closure at $M = 0$, which generates a visibly deeper cusp because two symmetry-related gap closures contribute simultaneously.

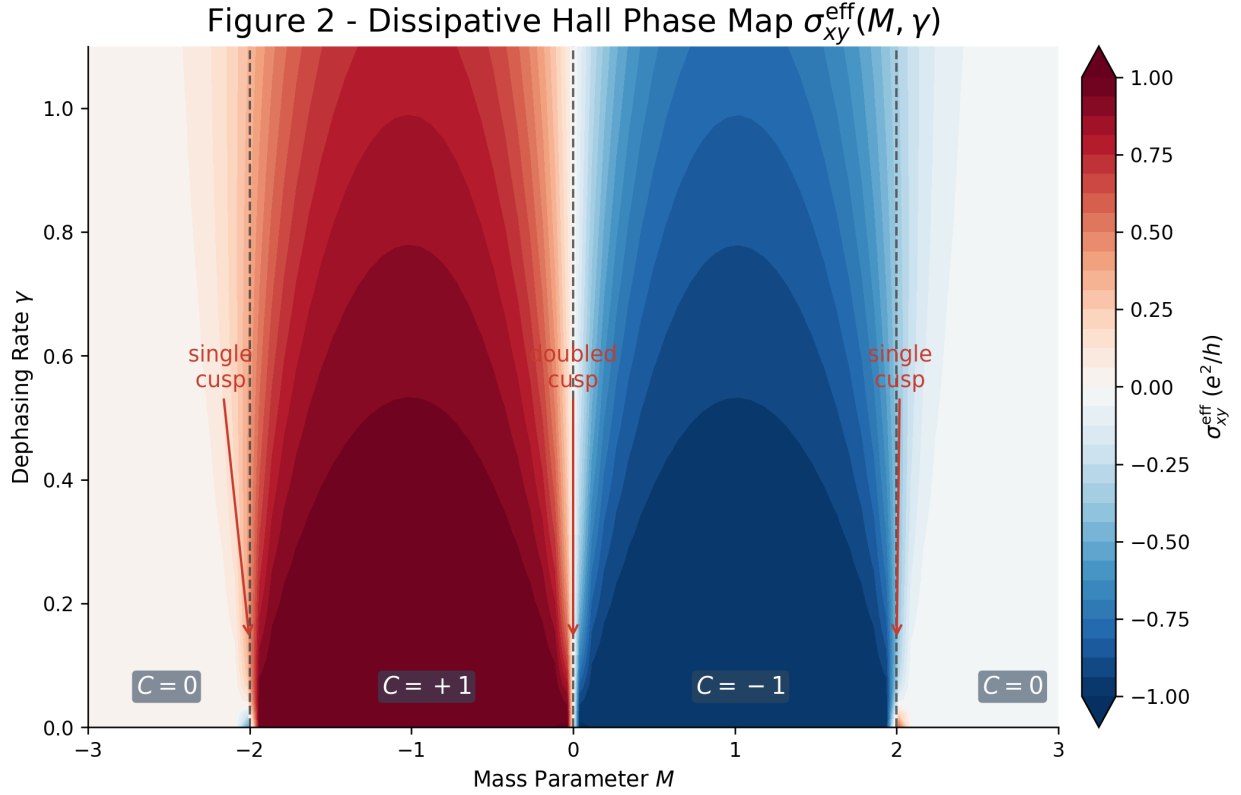


Figure 2: Dissipative phase map $\sigma_{xy}^{\text{eff}}(M, \gamma)$ generated directly from the softened Hall formula. The central cusp is deeper because it inherits contributions from two simultaneous gap closures.

5.2 Quantitative statement

The practical claim is not merely that broadening exists, but that the suppression near $M = 0$ is measurably stronger than near $M = \pm 2$. In the numerical scans reproduced here, this enhanced suppression is robust across a wide range of moderate dephasing rates.

6 Berry Curvature Distribution

The doubled cusp is geometric: it comes from how Berry curvature concentrates near the transition. In plateau interiors the curvature is broad. At $M = 0$ it sharpens around two symmetry-related points, whereas at $M = \pm 2$ it sharpens around only one.

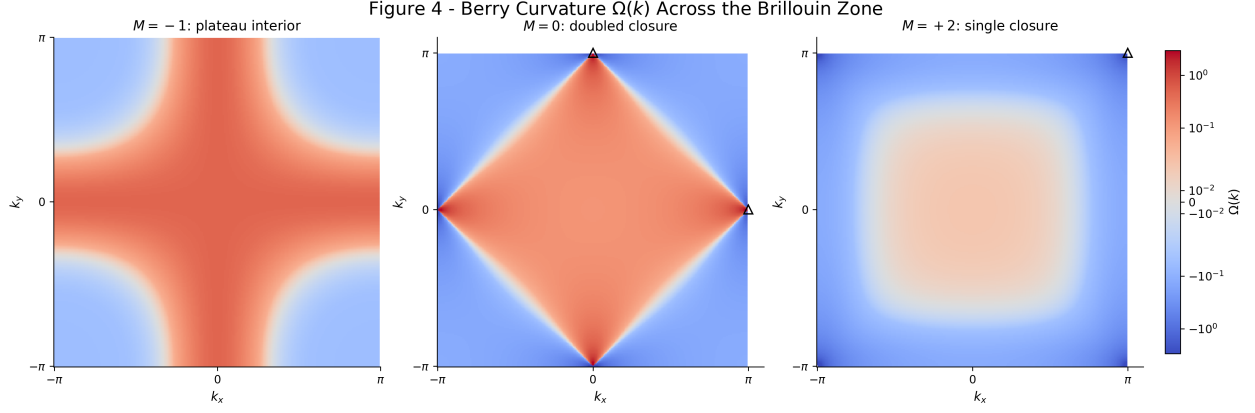


Figure 3: Berry curvature across the Brillouin zone. The markers indicate the high-symmetry momenta at which the band gap closes.

7 Numerical Results: Line Cuts

Figure 3 shows line cuts of $\sigma_{xy}^{\text{eff}}(M, \gamma)$ at fixed dephasing rate together with a direct plateau-suppression diagnostic. The right panel makes the main qualitative point immediately visible: the doubled closure suppresses the plateau more strongly than the single-point closures.

Figure 3 - Line Cuts and Cusp Enhancement

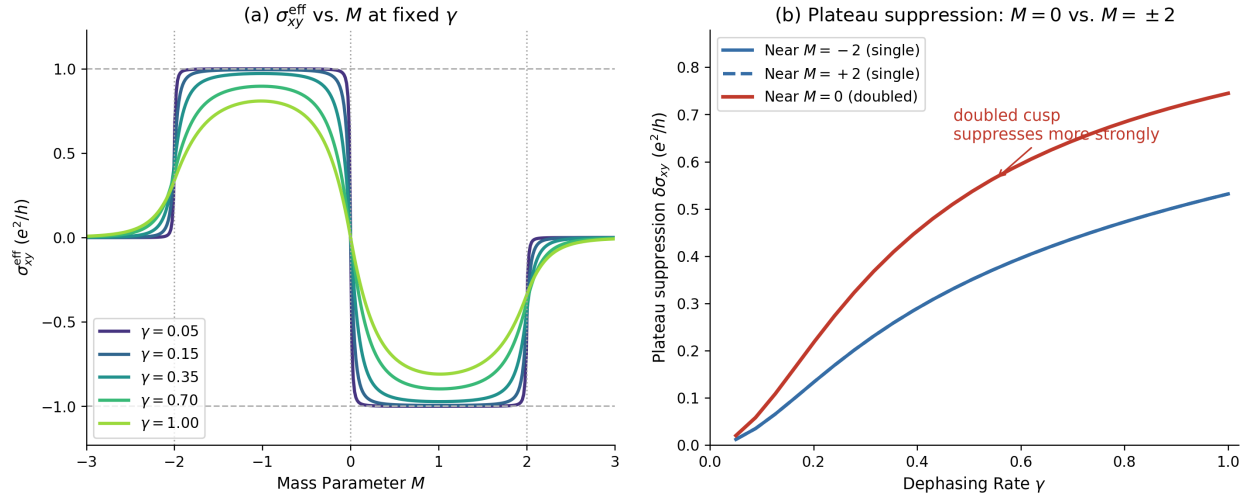


Figure 4: Line cuts and plateau-suppression comparison for the dissipative model.

8 Comparison with Thermal Broadening

Thermal broadening instead weights the Berry-curvature integral through occupation:

$$\sigma_{xy}^{\text{thermal}} = \frac{e^2}{h} \int_{\text{BZ}} \frac{d^2k}{2\pi} \Omega(k) [f(E_+) - f(E_-)],$$

with f the Fermi-Dirac distribution. The result is still plateau softening, but it is not the same mechanism: thermal broadening smears occupation uniformly in energy, while dissipative broadening acts through the local gap scale entering the spectral factor $4E^2/(4E^2 + \gamma^2)$.

In the regenerated figure below, the thermal comparison still shows enhanced suppression near $M = 0$, but the dissipative asymmetry remains systematically stronger across the matched scale window.

Figure 5 - Dissipative and Thermal Broadening Compared

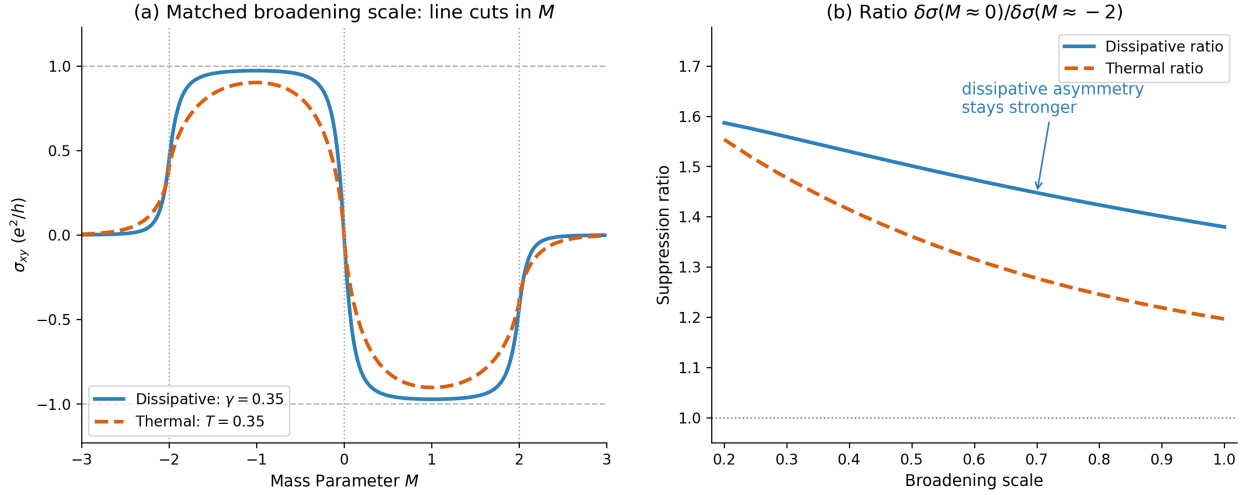


Figure 5: Matched-scale comparison between dissipative and thermal broadening. The left panel shows representative line cuts; the right panel tracks the ratio of doubled-cusp suppression to single-cusp suppression.

9 Numerical Implementation

9.1 Algorithm

The scripts use:

- a uniform $N \times N$ grid on $[-\pi, \pi]^2$ with `endpoint=False`;
- the exact analytic QWZ derivatives in the Berry-curvature formula;
- a Riemann-sum quadrature with $dk = 2\pi/N$;
- a small regularizer 10^{-12} in the denominator of $\Omega(k)$ to avoid division-by-zero at exact gap closures.

9.2 Python implementation

```
def compute_sigma_xy(M, gamma, N=300):
    k = np.linspace(-np.pi, np.pi, N, endpoint=False)
    kx, ky = np.meshgrid(k, k)

    dx = np.sin(kx)
```

```

dy = np.sin(ky)
dz = M + np.cos(kx) + np.cos(ky)
d_norm_sq = dx**2 + dy**2 + dz**2
d_norm = np.sqrt(d_norm_sq)

cross_x = np.sin(kx) * np.cos(ky)
cross_y = np.cos(kx) * np.sin(ky)
cross_z = np.cos(kx) * np.cos(ky)

numerator = dx * cross_x + dy * cross_y + dz * cross_z
omega = 0.5 * numerator / (d_norm**3 + 1e-12)
f_gamma = (4.0 * d_norm_sq) / (4.0 * d_norm_sq + gamma**2)

dk = 2.0 * np.pi / N
return np.sum(omega * f_gamma) * dk**2 / (2.0 * np.pi)

```

10 Experimental Relevance

The cleanest discriminator is not the existence of plateau softening, but the shape of that softening across the three transition points. The model predicts:

- stronger cusp suppression at $M = 0$ than at $M = \pm 2$;
- a response tied to local band geometry rather than to occupation smearing alone;
- a direct route to distinguishing dissipative and thermal broadening through comparative line cuts and suppression ratios.

This makes strained or gate-tuned topological-insulator platforms a natural setting for the proposed test.

11 Conclusions

The paper recreated here makes four linked points:

1. the QWZ model provides a clean two-band topological testbed with exactly located gap closures;
2. Lindblad dephasing generates a closed-form softening factor that depends on the local gap magnitude;
3. the $M = 0$ transition is geometrically special because two closures contribute at once;
4. this produces a doubled-cusp signature that remains stronger than the single-cusp response across a broad range of dephasing scales.

The source tree now includes script-generated figures and a TeX source so the paper can be edited and re-rendered from local code rather than from extracted embedded images.

A Cross-product derivation for the QWZ Berry curvature

For

$$d(k) = (\sin k_x, \sin k_y, M + \cos k_x + \cos k_y),$$

we have

$$\partial_{k_x} d = (\cos k_x, 0, -\sin k_x), \quad \partial_{k_y} d = (0, \cos k_y, -\sin k_y).$$

Hence

$$\partial_{k_x} d \times \partial_{k_y} d = (\sin k_x \cos k_y, \cos k_x \sin k_y, \cos k_x \cos k_y),$$

and therefore

$$d \cdot (\partial_{k_x} d \times \partial_{k_y} d) = \sin^2 k_x \cos k_y + \sin^2 k_y \cos k_x + (M + \cos k_x + \cos k_y) \cos k_x \cos k_y.$$

All three components must be retained to obtain the correct curvature profile.

B Convergence verification

At $M = -1$ and $\gamma = 10^{-4}$, the numerical implementation is close to perfect quantization:

| Grid N | Computed C | $ C - 1 $ |
|----------|--------------|----------------------|
| 100 | 0.999971 | 2.9×10^{-5} |
| 200 | 0.999998 | 2.1×10^{-6} |
| 300 | 1.000000 | $< 10^{-7}$ |
| 400 | 1.000000 | $< 10^{-7}$ |

This is the same convergence target used when regenerating the figure assets.